Hydrodynamics at large baryon densities: Understanding proton versus anti-proton v_2 and other puzzles

J. Steinheimer* and V. Koch
Lawrence Berkeley National Laboratory, 1 Cyclotron Road, Berkeley, California 94720, USA

M. Bleicher
Institut für Theoretische Physik, Goethe-Universität, Max-von-Laue-Str. 1, D-60438 Frankfurt am Main, Germany and Frankfurt Institute for Advanced Studies (FIAS), Ruth-Moufang-Str. 1, D-60438 Frankfurt am Main, Germany
(Received 22 August 2012; published 18 October 2012)

We study the importance of the initial state, baryon stopping, and baryon number transport for the dynamical evolution of a strongly interacting system produced in heavy ion collisions. We employ a hybrid model, which combines the fluid dynamical evolution of the fireball with a transport treatment for the initial state and the final hadronic phase. We present results for collisions at beam energies from $\sqrt{s_{NN}} = 7.7$ to 200 GeV. We study various observables such as the centrality dependent freeze-out parameters, the nonmonotonic behavior of effective slope parameter parameter with particle mass as well as the apparent difference in particle and antiparticle elliptic flow. Our results are in reasonable agreement with the available data. We find that the propagation of the baryon-number current in the hydrodynamic evolution as well as the transport treatment of the hadronic phase are essential for reproducing the experimental data.

DOI: 10.1103/PhysRevC.86.044903 PACS number(s): 25.75.Ag, 25.75.Ld, 24.10.Nz, 24.10.Lx

I. INTRODUCTION

Over the last decades many experimental programs at the Brookhaven National Laboratory and CERN facilities have been devoted to finding signals of a new state of matter, the quark gluon plasma (QGP), by means of relativistic heavy ion collisions. These experiments have produced a wealth of data including particle ratios and yields, transverse and longitudinal momentum spectra as well as the coefficients of a Fourier decomposition of the transverse flow patterns [1–16]. Several observations at the BNL Relativistic Heavy Ion Collider (RHIC) and CERN Large Hadron Collider (LHC) indicate that a strongly coupled QGP (sQGP) dominates the dynamical evolution [17–24]. In addition the energy dependencies of various observables, such as the K/π ratio, already show anomalies at low SPS energies which might be related to the onset of deconfinement and chiral symmetry restoration at lower energies [15,16]. While these are intriguing observations, experience has taught us that the interpretation of experimental results and their relation to the deconfinement phase transition is often ambiguous and extensive model studies are required to understand the numerous observables.

In order to study the physics of heavy ion collisions many models have been developed which address specific aspects of the these reactions. For example, hadron ratios are well described by thermal models which employ a hadronic resonance gas at a fixed temperature and chemical potential for the description of particle yields. The study of transverse and elliptic flow observables require more complex models: at the lowest energies hadronic transport, including the effects of hadronic potentials/interactions (see, e.g., [14,25–29]) are applied, while at the highest RHIC and LHC energies a description of the system in terms of fluid dynamics seems to be successful [30–37]. Since it is desirable to obtain a more comprehensive picture of the whole dynamics of heavy ion reactions, various so called hybrid approaches have been developed during the last years [38]. In these models one commonly uses initial conditions that are calculated in a non equilibrium model which are followed by an ideal or viscous hydrodynamic evolution. For the late stage of the collision a kinetic approach is more appropriate and, therefore, subsequent to the hydrodynamic evolution a transport model solving the Boltzmann equation is used for the description of the freeze-out stage [32,33,39–45]. Alternative approaches couple a partonic phase to a hadronic transport model [46–48]. As each phase may contribute considerably to final state observables, the interpretation of experimental results and their relation to the deconfinement phase transition are often a difficult task, and the contributions of the different phases need to be evaluated thoroughly.

The purpose of this paper is to study heavy ion collisions within the framework of one such hybrid model, the so-called UrQMD hybrid model [49] with the aim to re-evaluate some of the commonly accepted interpretations of various observables. Specifically we will address the centrality dependence of freeze-out parameters, transverse momentum spectra as well as antiparticle elliptic flow at low energies.

This paper is organized as follows. First we briefly introduce the hybrid model. Next we discuss particle production and transverse spectra obtained with the model. In the final section we present our results for the elliptic flow of particles and antiparticles with an emphasis on the difference between proton and anti-proton flow.

*jsfroschauer@lbl.gov

II. THE HYBRID MODEL

The UrQMD hybrid model combines the advantages of a hadronic transport model with an intermediate hydrodynamical stage for the hot and dense phase of a heavy ion collision. The UrQMD model [25,26] (in its cascade mode) is used to calculate the initial state of a heavy ion collision for the hydrodynamical evolution [50]. This is done to account for the nonequilibrium dynamics in the very early stage of the collision. The coupling between the UrQMD initial state and the hydrodynamical evolution happens at a time $t_{\rm start}$ when the two Lorentz-contracted nuclei have passed through each other:

$$t_{\rm start} = \frac{2R}{\sqrt{\gamma_{\rm c.m.}^2 - 1}}, \tag{1}$$

where $\gamma_{\rm c.m.}$ is the center-of-mass frame Lorentz factor and R is the radius of the nucleus. At this starting time all initial collisions have happened. It is further the earliest time at which local thermodynamical equilibrium may be achieved. At this time the energy, baryon number and momenta of all particles within UrQMD are mapped onto the spatial grid of the hydrodynamic model by representing each hadron by a Gaussian of finite width $\sigma = 1$ fm. In this approach the effects of event-by-event fluctuations and stopping of energy and baryon number density in the initial state are naturally included.

The full $(3+1)$-dimensional, one fluid, ideal hydrodynamic evolution is performed using the SHASTA algorithm [51,52]. We solve the equations for the conservation of energy and momentum:

$$\partial_\mu T^{\mu\nu} = 0 \tag{2}$$

and for the conservation of the baryonic current,

$$\partial_\mu N^\mu = 0. \tag{3}$$

Here $T^{\mu\nu}$ is the relativistic energy momentum tensor,

$$T^{\mu\nu} = (\epsilon + p)u^\mu u^\nu - g^{\mu\nu} p \tag{4}$$

and N^μ the baryonic current

$$N^\mu = n\, u^\mu. \tag{5}$$

The above partial differential equations are solved on a three-dimensional spatial Eulerian grid with fixed position and size $\delta x = 0.2$ fm in the computational frame. The local rest frame is defined as the frame where $T^{\mu\nu}$ has diagonal form (i.e., all off-diagonal elements vanish), also known as the Landau frame. To close the set of equations an equation of state (EoS), the pressure as function of energy and baryon number density $p(\epsilon, n)$ needs to be specified. In the following we will use an EoS that corresponds to an hadron resonance gas. This is convenient as it includes the same degrees of freedom as the UrQMD model, which essentially allows us to study the effect of local equilibrium on the different observables. Previous investigations have shown that different equations of state only lead to insignificant differences in the results [53,54].

To transfer all particles back into the UrQMD model, an approximate iso-eigentime transition is chosen (see [55] for details). To this end we apply the Cooper-Frye prescription [56] to individual transverse slices, of thickness $\Delta z = 0.2$ fm, at a time-like transition hypersurface. The transition time for a given slice is determined by the time when the energy density ε in every cell of this slice has dropped below five times the nuclear ground state energy density, i.e., below $\sim$730 MeV/fm^3. As a result we obtain a longitudinal iso-eigentime transition with an almost rapidity independent maximum switching temperature for beam energies above $\sqrt{s_{NN}} \approx 10$ GeV.[1] In a given slice the hydrodynamic fields are transformed to particle degrees of freedom via the Cooper-Frye equation:

$$E\,\frac{dN}{d^3p} = g_i \int_\sigma f_i(x,\, p)\; p^\mu\; d\sigma_\mu \tag{6}$$

on an isochronous time-like hypersurface in the computational frame [the hypersurface normal is $d\sigma_\mu = (d^3x, 0, 0, 0)$]. Here $f_i(x, p)$ are the distribution functions and g_i the degeneracy factors for the different particle species i, which in our case are given by the appropriate Bose or Fermi distributions. The particle distributions explicitly depend on the local values of the temperature T and baryon chemical potential μ_B. T and μ_B are obtained by converting the local energy- and baryon-densities via the equation of state.

The above transition procedure conserves baryon number, electric charge, the total net strangeness and the total energy on an event-by-event basis. After the particles are created they evolve according to a hadronic cascade (UrQMD) where final rescatterings and decays are calculated until all interactions cease. A more detailed description of the hybrid model including parameter tests and results can be found in Ref. [49].

A. Particle yields and the temperature distribution

The description of particle production in heavy ion collisions using statistical methods, such as thermal models [57–59] and fluid dynamical models with a sudden freeze-out, are usually based on the assumption that for a given incident beam energy chemical freeze-out occurs at a fixed temperature and chemical potential. As we have discussed above (see also [54]) we transform full transverse slices at a given time t, using the Cooper-Frye prescription. This implies that contrary to an isothermal transition particles are emitted over a range of temperatures/densities. While this may no be a standard procedure it has been shown in several publications [49,60–64] that this hybrid model is very well suited to describe particle ratios and yields over a wide range of energies. In addition, recent comparisons of an isothermal $3+1$-dimensional hypersurface [65] indicate that deviations only occur at large transverse momenta ($p_\perp > 1$ GeV), corresponding in our freeze-out prescription to very cold and fast cells which are being treated as equilibrated for an extended period of time. Since all

[1] This ensures that all cells have passed through a potential mixed phase of the equation of state and the effective degrees of freedom at the transition are hadronic. As mentioned above we use a hadron resonance gas EoS for our present study which does not include a phase transition. However, we could include an EoS with a phase transition, even though most bulk observables have shown to be insensitive on the specific choice of the EoS [53–55].

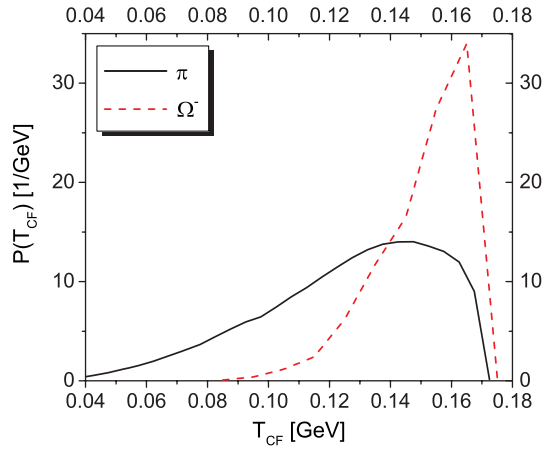

FIG. 1. (Color online) Probability distributions $P(T_{\rm CF})$ for pions (black solid line) and Ω^-'s (red dashed line) to be produced from a cell with a give temperature $T_{\rm CF}$. The results shown are for central collisions of Pb nuclei with a beam energy of $\sqrt{s_{NN}} = 17.3$ GeV.

observables we discuss in this paper are mainly determined at lower momenta our results hold also for the isothermal case. The comparison also implies that both dynamical descriptions, transport and hydrodynamics, give equivalent results for the fireballs expansion in the transition region considered.

Figure 1 shows the resulting probability distributions $P(T_{\rm CF})$ for pions and Ω^-'s to be produced from a cell with a given temperature $T_{\rm CF}$. Note that $T_{\rm CF}$ is the temperature that enters into the Cooper-Frye equation (6). The results shown are for central collisions of Pb nuclei at a center-of-mass energy of $\sqrt{s_{NN}} = 17.3$ GeV. One can clearly see that the pions, due to their smaller mass, are generally emitted/produced at lower temperatures than the Ω's. In other words, because we allow for emission from all local temperatures the heavier particles are preferentially emitted from regions of higher temperatures. The lower plot of Fig. 2 illustrates how the average value of $T_{\rm CF}$ changes as a function of the particle mass for different hadron species. Results for Pb + Pb/Au + Au collisions at $\sqrt{s_{NN}} = 17.3$ and 200 GeV are shown. One observes a clear trend of increasing $T_{\rm CF}$ with the particle mass, as shown explicitly for the pion and Ω.

We also observe a mass dependence of the average transverse flow $\langle v_\perp \rangle$, defined as the average of the hydrodynamical radial flow velocity over the production points of the particles. Results for the different particle species are depicted in the upper part of Fig. 2. It is clear that hot and dense cells usually have a smaller flow velocity because they tend to be located at the center of the collision zone. The colder cells are more peripheral and therefore have acquired more flow.

At lower beam energies, the finite baryon density (chemical potential) plays an important role. Because the proton has a large chemical potential, it is much more abundant at lower temperatures than it's anti-particle, resulting in a distinctly different value of $\langle T_{\rm CF} \rangle$, defined as the average of temperatures over the production points of the particular particles. Figure 3 depicts the averaged ratio of anti-protons over protons, taken at the last time step of an Au + Au collision at a beam energy of $\sqrt{s_{NN}} = 11.5$ GeV, $\bar{p}/p = \exp(-2\mu_B/T)$, as a

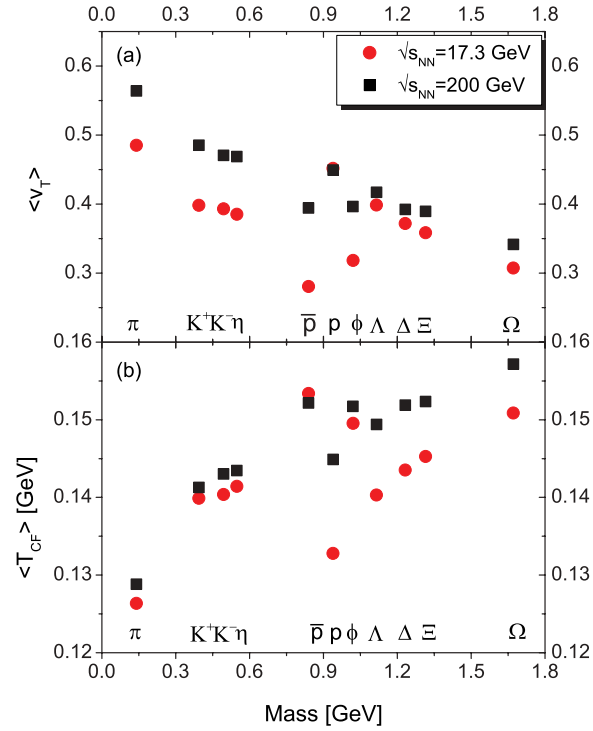

FIG. 2. (Color online) The average transverse flow velocity $\langle v_\perp \rangle$ (a) and $T_{\rm CF}$ (b) at the Cooper Frye transition, as a function of the particle mass for different hadron species. Results for most central Pb + Pb/Au + Au collisions at $\sqrt{s_{NN}} = 17.3$ (black squares) and 200 GeV (red circles) are shown. Note the anti-proton mass has been shifted for visibility.

function of radius (red dashed line). Clearly the $\bar{p}/p$ ratio is largest in the center of the collision zone where the radial flow has its minimum. The transverse flow velocity $v_\perp$ of the hydrodynamic fluid (black solid line), extracted from our hydrodynamical calculation, increases linearly with the

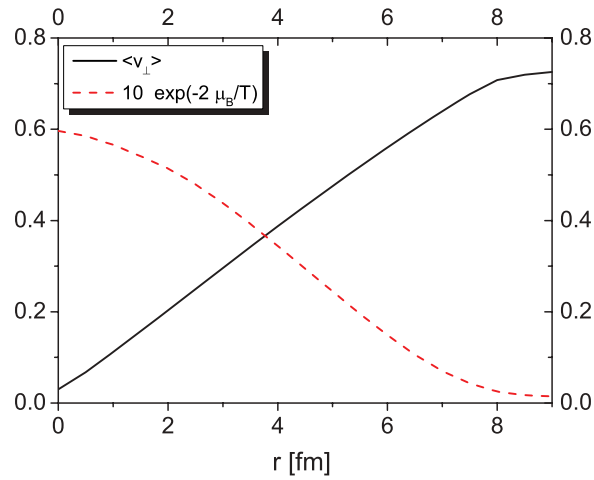

FIG. 3. (Color online) Average transverse hydrodynamical flow velocity (black solid line) and the scaled ratio of protons over anti-protons $\approx \exp(-2\mu_B/T)$ (red dashed line) as a function of transverse radius. The results shown are for the central transverse plane at the end of a hydrodynamical calculation for Au + Au at $\sqrt{s_{NN}} = 11.5$ GeV.

distance from the center of the collision. Consequently the anti-protons will acquire a smaller average transverse flow as compared to the protons, even though their transverse velocity for any given r is identical. The conclusion that protons and anti-protons acquire a different average flow velocity also holds true for an iso-thermal transition because the ratio $\bar{p}/p$ will in general not be constant over the hypersurface. The quantitative difference however might very well depend on the definition of the transition hypersurface. It is therefore interesting to extend the current investigation to different hypersurfaces.[2]

Note that the same argument should also hold for other conserved charges, such as strangeness and the third component of the isospin. Because the colliding nuclei have more neutrons than protons the third component of the isospin is finite, and *negative* in the produced fireball. Therefore, we expect the ratio π^+/π^- to depend on the radius similar to the $\bar{p}/p$ ratio, which in consequence will lead to a different transverse flow velocity of π^+ compared to π^-. However the effect will be much weaker for pions since it depends on the ratio of the fugacities $\exp(-2\mu_I/T)$ and the isospin chemical potential is considerably smaller then the baryon chemical potential $-\mu_I < \mu_S < \mu_B$. For the top SPS energy a thermal model analysis found values of: $\mu_I = -5.0$ MeV, $\mu_S = 71.1$ MeV and $\mu_B = 266 \pm 5$ MeV [66].

B. Centrality dependence of freeze-out parameters

An ideal fluid dynamical treatment of the expansion implies that for a given freeze-out criterion the particle abundances are fixed by the total entropy per baryon (S/A) produced in the very early stage of the collision, since the subsequent expansion is isentropic.

In all models used to describe the properties of the early stage of an heavy ion collision (Glauber model, geometrical overlap, hadronic transport) the initial state is defined by the total energy and baryon number deposited in the fireball. In a Glauber model [1,10,67] the energy deposition in the transverse plane is proportional to the number of wounded nucleons:

$$\begin{aligned} &e(x,y;\tau_0) \\ &= K\left\{T_A\left(x+\frac{b}{2},y\right)\left[1-\left(1-\frac{\sigma T_B\left(x-\frac{b}{2},y\right)}{B}\right)^B\right]\right. \\ &\left.+T_B\left(x-\frac{b}{2},y\right)\left[1-\left(1-\frac{\sigma T_A\left(x+\frac{b}{2},y\right)}{A}\right)^A\right]\right\}, \end{aligned} \quad (7)$$

where T_A and T_B are the nuclear thickness functions of the incoming nuclei A and B, σ is an energy dependent cross section, and K is a proportionality factor. If we further assume that the initial baryon density is proportional to the initial energy density [10],

$$n(x,y;\tau_0) = C(\sqrt{s_{NN}})\cdot e(x,y;\tau_0), \quad (8)$$

the initial energy per baryon $(E/A)(r)$ as a function of the transverse radius is a constant which only depends on the collision energy. At the same time the energy and baryon densities drop rather quickly as a function of radius r. Since E/A is constant, a decreasing energy density implies that the entropy per baryon S/A must vary as a function of r as the entropy density in general does not scale with the energy density,

$$\frac{s(x,y;\tau_0)}{e(x,y;\tau_0)} \neq \text{constant}. \quad (9)$$

In addition the average energy density varies as a function of centrality. Since E/A is constant we also expect a centrality dependence of the total entropy per baryon.

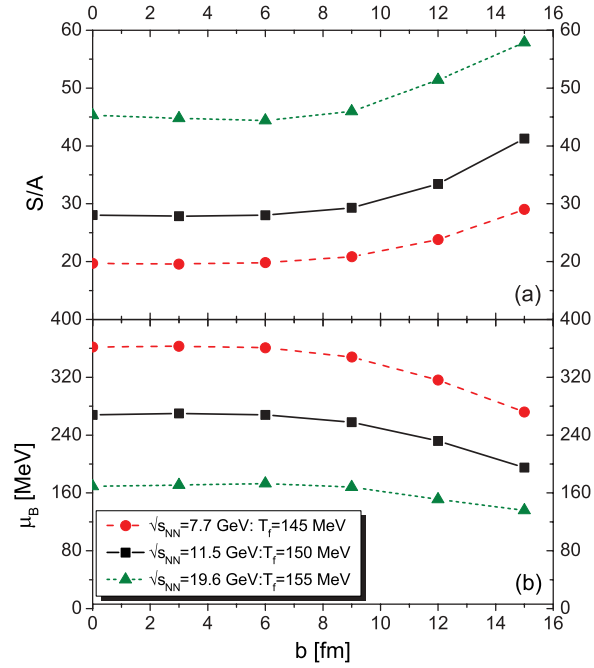

FIG. 4. (Color online) (a) Centrality dependence of the entropy per baryon produced. (b) Corresponding baryon chemical potential for a given fixed temperatures T_f.

Figure 4 exemplifies the effects of the initial geometry on the final chemical composition of the fireball. Figure 4(a) shows the total entropy per baryon produced in collisions of Au nuclei at energies of $\sqrt{(s_{NN})} = 7.7$–19.6 GeV, as a function of impact parameter b. The entropy per baryon is calculated, averaging over 1000 UrQMD initial state events (although it has been shown that S/A does only vary weakly on an event-by-event basis [50]). A hadron resonance gas (HRG) equation of state is used to estimate the values for the entropy per baryon as it best resembles the active degrees of freedom at the particle freeze-out. We find that the produced S/A increases with the impact parameter, simply because of the different initial geometry. Using the HRG we can determine the baryonic chemical potential μ_B, corresponding the value of S/A when fixing the temperature to any given value T_f. For

[2]For these further studies we need to apply a hypersurface finder for our full $3+1$D calculation including local density fluctuations. Such a tool has recently been developed [65] and can be applied for future studies.

the thermal models of particle production this temperature corresponds to the chemical freeze-out temperature. The resulting values for μ_B are shown in Fig. 4(b) as a function of b. It is clear that μ_B decreases with increasing b. We note that such an effect has been observed in experiment [68], where thermal fits to different centrality selections show a decreasing μ_B with centrality which is of comparable magnitude to our results shown here. This observation indicates that the systems created in heavy ion collisions of fixed energy but varying centrality cannot be characterized by single values for the thermal parameters.

III. THE SLOPE PARAMETER

After discussing the integrated yields, let us next discuss the transverse momentum spectra, which are considered to be more sensitive to the kinetic decoupling temperature, T_{th}, and transverse flow than average yields. Taking Eq. (6) and neglecting any flow the transverse momentum distribution (for $p_z \to 0$) is given by

$$\frac{1}{m_\perp}\frac{dN_i}{dm_\perp dy} \propto m_\perp (\exp((m_\perp - \mu_i)/T) \pm 1)^{-1} \qquad (10)$$

with the transverse mass $m_\perp = \sqrt{(m_i^2 + p_\perp^2)}$. The negative slope of $\log(\frac{1}{m_\perp^2}\frac{dN_i}{dm_\perp dy})$ gives the so called *effective* temperature $T_{\rm eff}$ [69,70], which, however, does not correspond to the actual kinetic decoupling temperature T_{th} since the spectra are blue shifted due to transverse flow. To account for the flow the effective temperature can be related to the kinetic decoupling temperature by $T_{\rm eff} = T_{th} + m_i \langle v_\perp \rangle^2$.

These type of fits to experimental data typically result in a nonmonotonic behavior in $T_{\rm eff}$ as a function of particle mass, which cannot be accounted for with a fixed temperature freeze-out [30,71,72]. Note that in our calculation we cannot directly extract a value for the kinetic freeze-out temperature T_{th}, because we treat the kinetic decoupling as a dynamical process within the UrQMD transport model.

In addition to flow effects resonance decays as well as scattering processes in the hadronic phase affect the extracted value of $T_{\rm eff}$ as a function of mass [30,69,73,74]. To successfully interpret the experimental results one, therefore, has to disentangle the different contributions to the transverse spectra in a consistent approach.

Using the UrQMD hybrid model we can disentangle all the important contributions and explore what information about the hot and dense phase can be extracted from the spectra. Figure 5 shows the midrapidity ($|y| < 0.5$) $m_\perp$ spectra of pions protons and Ω's, divided by $m_\perp^2$, for the most central collisions of Pb nuclei at $\sqrt{(s_{NN})} = 17.3$ GeV. We compare the final spectra (black squares) with the ones obtained directly after the Cooper Frye transition, without any UrQMD final state, where we either let all resonances decay at the transition (red circles labeled as 'no afterburner') or do not allow for resonance decays at the transition. (green triangles labeled as 'no resonance feed down'). The two latter cases are interesting to distinguish because they show the effect of the final state rescattering on the momentum distribution functions,

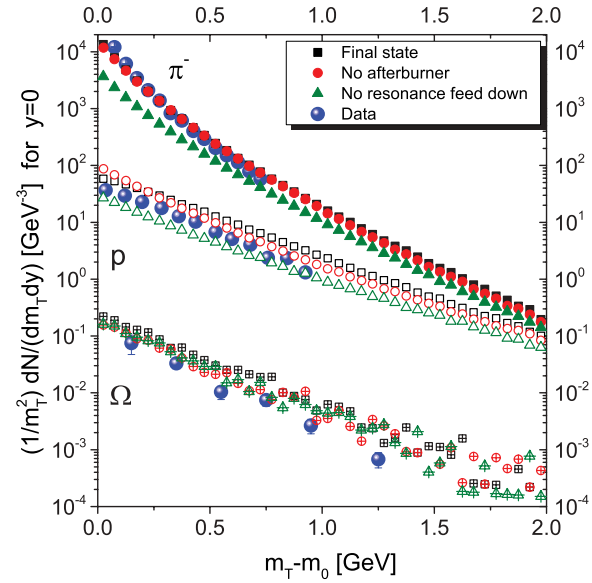

FIG. 5. (Color online) Transverse mass distributions of pions protons and Ω's at midrapidity $|y| < 0.5$, divided by $m_\perp^2$, for most central collisions of Pb nuclei at $\sqrt{s_{NN}} = 17.3$ GeV. We compare the distributions from the hybrid model extracted at the final state (black squares) with those directly at the Cooper-Frye transition with (red circles) and without (green triangles) resonance decays. Data from 1 the NA49 experiment are depicted as large blue circles [75–77].

indicating that the final hadronic state is not a mere decay of resonances. For comparison we also show the experimental data by the NA49 collaboration [75–77] as blue circles.

We see that the spectra of both pions and protons are significantly modified due to hadronic interactions and resonance decays. We further find deviations of the spectra from an exponential shape already at the Cooper-Frye transition, when no resonance decays are taken into account. This is a result of the blue shift due to the finite flow already present at the transition, as shown in Fig. 2, and is also connected to our freeze-out treatment of summing up thermal distributions with different temperatures, which was first discussed in Refs. [78–80].

We note that similar modifications of the $p_\perp$ spectra due to final state interactions were obtained in an earlier calculation [30], where the UrQMD model was used for the final state of a hydrodynamical calculation with an *isothermal* freeze-out.

In both calculations, ours as well as that of Ref. [30], only the Ω does not change noticeably during the afterburner phase because of it's small hadronic cross section. Furthermore there are no resonance states in the model that contribute to the Ω spectrum.

Resonances change the momentum spectra mainly at low momenta, because of the restricted phase space of the decays and their effects should become negligible at some point. This is demonstrated in Fig. 6 where we show the ratio of the transverse mass spectra after the resonance decays to those before the decays for four different particles. The strongest modification of the spectra is observed for the pions and protons: they are enhanced by a factor of three at low momenta. However, we find that the effect of resonances

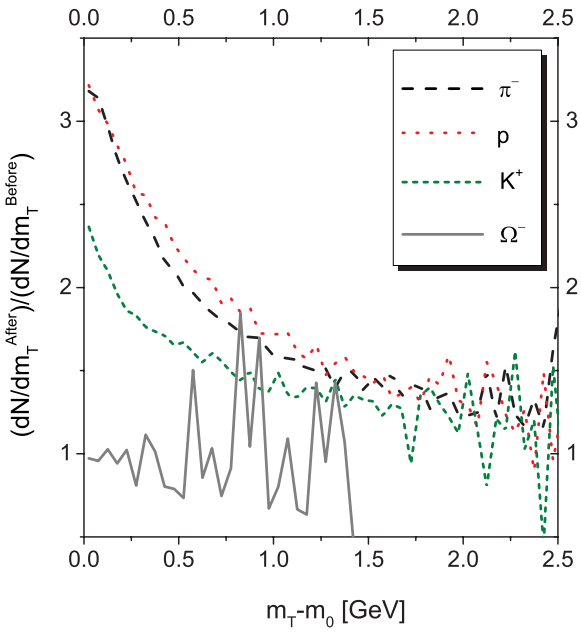

FIG. 6. (Color online) Ratios of transverse mass distributions after to before resonance decays, shown for pions protons kaons and Ω's, as a function of $m_\perp$.

is still considerable even for $m_\perp - m_0 > 1$ GeV, which is consistent with previous works [69,73]. Therefore, it is questionable that an exponential fit below a transverse mass of $m_\perp - m_0 < 1$ GeV is in any way justified, and even at higher transverse masses one would expect small deviations from the exponential form.

In Fig. 7 we show the exponential fits to spectra obtained with the hybrid model over a mass range of

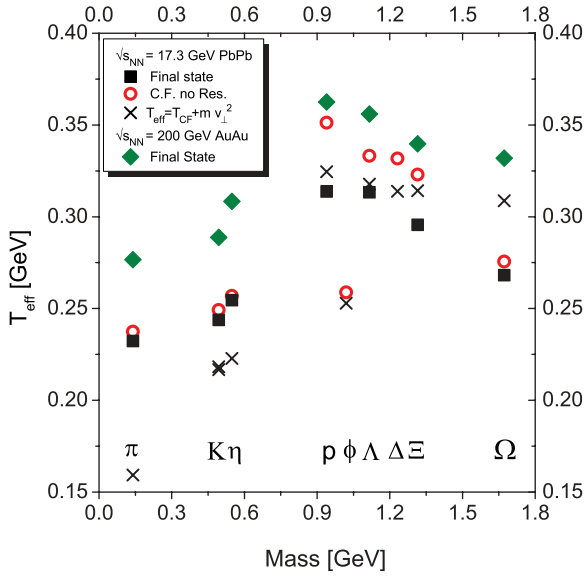

FIG. 7. (Color online) Extracted slope parameters $T_{\rm eff}$ from the hybrid model for different particle species. We compare final state results (full symbols) with results obtained at the Cooper-Frye transition without resonance decays (open symbols).

$1 < m_\perp - m_0 < 2$ GeV. The filled symbols correspond to fits of final state spectra, including resonance decays and the UrQMD afterburner, for most central PbPb/AuAu collisions at $\sqrt{(s_{NN})} = 17.3$ GeV (black squares) and $\sqrt{(s_{NN})} = 200$ GeV (green diamonds) GeV. The red open circles correspond to fits to spectra directly after the Cooper-Frye transition without resonance decays. One clearly observes a nonmonotonic behavior in the effective slope parameter as a function of the particles mass. It was shown in earlier publications [30] that such a behavior can also be accounted for when UrQMD is used as the afterburner for an isothermal transition. In that work the scattering processes in the transport phase create a situation where the actual dynamical decoupling takes place over a range of densities/temperatures leading to results comparable with our study. As indicated before, the hydrodynamical and transport description give equivalent results over a certain range of densities and our non-isothermal transition is generally not ruled out. The question whether there is a sharp transition, as in the isothermal case, or a certain transition region may be further investigated by carefully studying the spectra of the ϕ and Ω, which emerge at the transition from the collective phase to the hadronic phase and do not rescatter significantly in the transport phase. Their final state observables, therefore, contain the information from the transition surface, without interference from the hadronic phase of the collision.

To estimate how well the approximation $T_{\rm eff} = T_{th} + m_i \langle v_\perp \rangle^2$, with $\langle v_\perp \rangle$ taken from Fig. 2, compares with our fit results, we plotted the simple estimates of $T_{\rm eff}$ as black crosses. They should be compared with the open red circles because we estimated the flow effect on $T_{\rm eff}$ at the Cooper-Frye transition where $T_{th} = T_{\rm CF}$, as we cannot explicitly extract T_{th} from our calculation. It is obvious that the simple formula fails to describe the slope parameter for most of the light mesons and works more reliably for the heavy baryons, indicating that the final hadronic stage is important for the complete description of final particle spectra.

IV. ELLIPTIC FLOW

The elliptic flow parameter v_2 has long been proposed as a probe for the properties of the hot and dense system created in a heavy ion collisions [1–4,7–9,11,81–83]. The elliptic flow parameter v_2 is defined as the coefficient of the second Fourier component of the azimuthal distribution of the emitted particles:

$$\frac{dN}{p_\perp dp_\perp d\Phi} = \frac{1}{2\pi}\frac{dN}{p_\perp dp_\perp}[1 + 2v_2(p_\perp)\cos(2\Phi) + 2v_4(p_\perp)\cos(4\Phi) + \cdots], \quad (11)$$

where the azimuthal angle $\Phi = \phi - \psi_{\rm RP}$ is measured with respect to the direction of the reaction plane, $\psi_{\rm RP}$

The average or integrated elliptic flow coefficient, $\bar{v}_2$, is defined as

$$\bar{v}_2 = \langle \cos[2(\Phi)] \rangle \quad (12)$$

and is given in terms of the azimuthal distribution as

$$\bar{v}_2 = \frac{\int dp_\perp \int_0^{2\pi} d\Phi \frac{dN}{dp_\perp d\Phi} \cos(2\Phi)}{\int dp_\perp \int_0^{2\pi} d\Phi \frac{dN}{dp_\perp d\Phi}} \tag{13}$$

$$= \frac{1}{N} \int dp_\perp \int_0^{2\pi} d\Phi \frac{dN}{dp_\perp d\Phi} \frac{p_x^2 - p_y^2}{p_\perp^2} \tag{14}$$

$$= \frac{1}{N} \left\langle \frac{p_x^2 - p_y^2}{p_x^2 + p_y^2} \right\rangle. \tag{15}$$

The integrated elliptic flow is related to the $p_\perp$ dependent elliptic flow by

$$\bar{v}_2 = \frac{\int dp_\perp v_2(p_\perp) \frac{dN}{dp_\perp}}{\int dp_\perp \frac{dN}{dp_\perp}}. \tag{16}$$

To calculate $\bar{v}_2$ in fluid dynamics one usually performs a Cooper-Frye freeze-out and then uses the above definitions.

Alternatively one can use the energy momentum tensor $T_{\mu\nu}$ and directly extract the flow anisotropy from the hydrodynamical computation [84,85]:

$$\bar{v}_{2,T} = \frac{\langle T_{xx} - T_{yy} \rangle}{\langle T_{xx} + T_{yy} \rangle} \tag{17}$$

$$= \frac{\int d^3r \int d^3p \frac{(p_x^2 - p_y^2)}{p_0} f(r, p)}{\int d^3r \int d^3p \frac{(p_x^2 + p_y^2)}{p_0} f(r, p)}. \tag{18}$$

Here, $f(r, p)$ is the phase space distribution, and T_{xx}, T_{yy} are the appropriate components of the energy momentum tensor. This prescription is different from the actual definition of $\bar{v}_2$ which is given by Eq. (14). It has an additional weighting of $p_\perp^2/p_0$ in front of $\frac{dN}{dp_\perp d\Phi}$. However, it was empirically found [84] that the pion elliptic flow can be related to $\bar{v}_{2,T}$ as $2\,\bar{v}_2 \approx \bar{v}_{2,T}$. Assuming that $v_2(p_\perp) \propto p_\perp$ and that $f(r, p)$ is represented by a Boltzmann distribution on can easily show that $\frac{3}{2}\,\bar{v}_2 \approx \bar{v}_{2,T}$. However, the distribution function for pions is considerably distorted by resonance decays and far from being of Boltzmann type, especially at small transverse momenta. This brings the factor relating the two definitions close to the observed value of 2.

In Fig. 8 we show results for the integrated $\bar{v}_2$ of different particle species, pions protons and anti-protons, as a function of time, extracted from the hydrodynamical phase of the hybrid model. For this calculation we used a non-fluctuating initial condition created by averaging 1000 UrQMD events of collisions of Au nuclei at an $\sqrt{s_{NN}} = 11.5$ GeV and an impact parameter of $b = 8$ fm. The symbols denote values of $\bar{v}_2$ extracted from sampling the Cooper-Frye equation on an isochronous hypersurface at each time step, hence representing the correct definition of $\bar{v}_2$. The lines represent values of $\bar{v}_{2,T}$ extracted from the hydrodynamical energy momentum tensor as described in equation (17). For the pion elliptic flow we used the full energy momentum tensor and multiplied $\bar{v}_{2,T}$ by a factor of 0.5 as suggested in Ref. [84] and one can observe a very good agreement of the methods. To extract the proton and anti-proton flow we used the partial energy momentum tensor of the protons and anti-protons and multiplied them by 2/3 as suggested above. The partial $T_{\mu\nu}$'s for protons and anti-protons

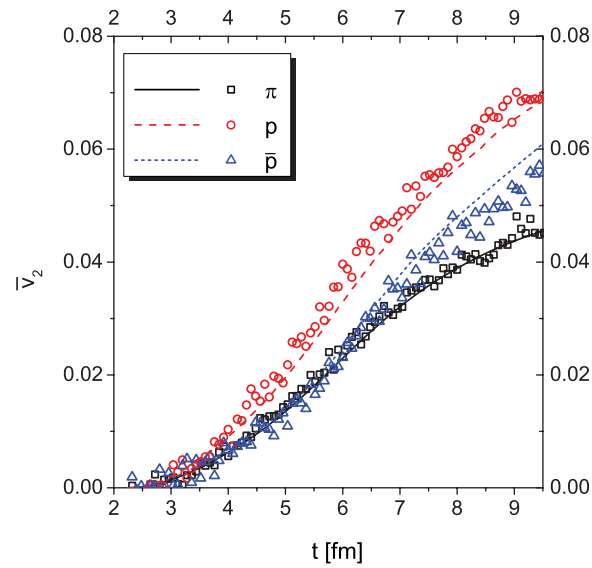

FIG. 8. (Color online) Elliptic flow as a function of time for an averaged UrQMD initial condition of two Au nuclei colliding at $\sqrt{(s_{NN})} = 11.5A$ GeV and an impact parameter of $b = 8$ fm. The lines correspond to $\bar{v}_2$ extracted using the energy momentum tensor Eq. (17), and the symbols denote results from a sampling of the Cooper-Frye equation.

are related simply by

$$T^{\bar{p}}_{\mu\nu} = \exp\left(-2\mu_B(x, y)/T(x, y)\right) \cdot T^{p}_{\mu\nu} \tag{19}$$

(μ_B and T being the baryon chemical potential and temperature, respectively).

The resulting proton and anti-proton $\bar{v}_2$'s are in reasonable qualitative agreement for both methods presented.

In either case we observe that the integrated elliptic flow of protons is systematically larger than that of the anti-protons. This difference is also observed in recent preliminary experimental data from the STAR Collaboration [86]. Below a collision energy of $\sqrt{s_{NN}} < 60$ GeV the measured elliptic flow of particles is considerably different from that of their antiparticles and the difference increases with decreasing beam energy and correspondingly increasing net baryon density. A recent transport calculation was able to explain such an effect qualitatively by the inclusion of mean field type nuclear potentials [87]. Our calculations, however, indicate that the average flow of, e.g., anti-protons is different from that of protons simply because their local 'weight', given by $\exp\left(-2\mu_B(x, y)/T(x, y)\right)$ in the evaluation of, e.g., Eq. (19), varies due to the finite net baryon density. As shown in Fig. 3 the ratio of $\bar{p}/p$ is large for the cells in the center of the collision which have a high temperature and small flow velocity, and it is small for the colder cell at the surface, which carry high flow velocities. As a result the average transverse flow for protons is larger than that for anti-protons resulting in a larger value for $\bar{v}_2$ of protons.

Let us next quantify the discussed difference in elliptic flow and investigate to which extent our result is modified when we apply the full hybrid model including event-by-event fluctuations, resonance decays as well as an afterburner stage. Figure 9 shows the difference of particle-antiparticle $\bar{v}_2$ of

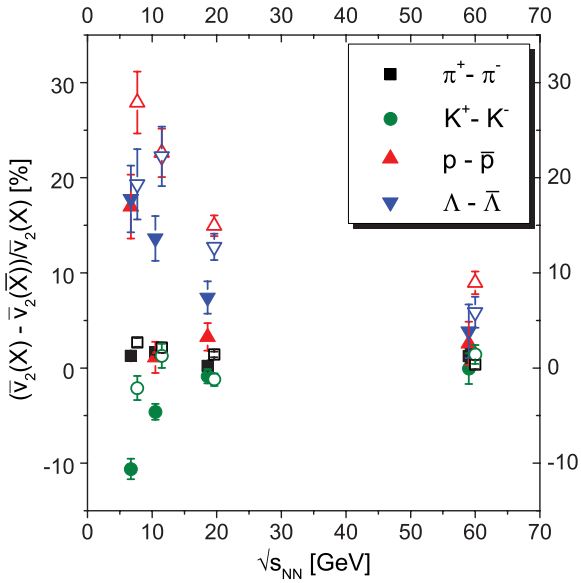

FIG. 9. (Color online) Difference of particle and antiparticle $\bar{v}_2$ as a function of beam energy for different particle species. The open symbols denote results at the Cooper-Frye transition while the full symbols represent results with the full UrQMD afterburner stage.

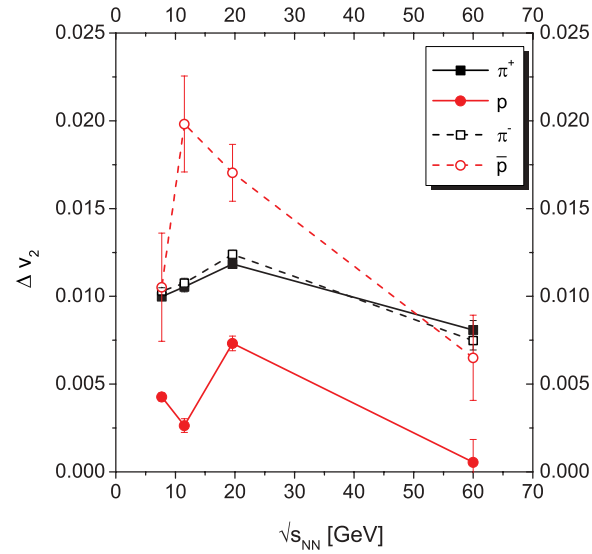

FIG. 10. (Color online) Effect of the final hadronic state on particle and antiparticle $\bar{v}_2$ as a function of beam energy. Δv_2 is defined as the gain of the elliptic flow coefficient obtained in the final transport phase: $\bar{v}_2^{\text{Final}} - \bar{v}_2^{\text{CF}}$.

different particle species as a function of $\sqrt{s_{NN}}$ for collisions of Au + Au nuclei at an impact parameter of $b = 8$ fm. In the plot the full symbols correspond to results obtained after the UrQMD final state while the open symbols denote results after the Cooper-Frye transition, including resonance decays. In general the difference in elliptic flow is most pronounced directly after the Cooper Frye transition out of the hydrodynamical evolution and is washed out by the subsequent UrQMD transport phase. For baryons we observe a considerable increase in the difference of $\bar{v}_2$ between particles and antiparticles with decreasing beam energy. The value of $\bar{v}_2$ is essentially the same for π^+ and π^-. For the kaons we observe a trend, which is opposite to the one found in data [86], showing that K^- $\bar{v}_2$ seems larger than that of K^+. However, this is only the case after the final UrQMD transport stage. Directly after the hydrodynamical evolution kaons appear to have the same flow. The observed phenomenon can therefore be interpreted as a natural result of a net density and a chemically equilibrated phase.

Many transport descriptions fail to even qualitatively describe the phenomenon because they lack certain interaction channels which are important at the energies considered here. For example the difference in the Kaon elliptic flow could be explained by missing strangeness exchange reactions in the final state. For the antiparticles the inclusion of all pair creation processes is important. Since antiparticles are very rare in low energy collisions, their flow is sensitive to their explicit interactions, i.e., annihilation and recreation, in the transport phase. At the highest beam energies a large number of antiparticles is produced at hadronization and regeneration has only a small effect on their abundance (seen in LHC data [88,89]). However when the beam energy is decreased, only few antiparticles are produced and the pair creation due to multi pion reactions becomes non negligible for the antiparticles bulk properties [90–93].

To illustrate the effect of the hadronic transport phase on the elliptic flow, in Fig. 10 we show the difference between the value of $\bar{v}_2$ in the final state to that obtained right after the Copper-Frye transition for protons, anti-protons and charged pions. Clearly, at low energies the value for $\bar{v}_2$ for anti-protons increases appreciably during the hadronic transport phase. This is simply an effect of the annihilation process. Anti-protons moving in the out-of-plane (y) direction encounter more protons to annihilate with than those moving in the in-plane (x) direction. Since there are many more protons than anti-protons, the annihilation only affects the anti-protons. Because the reverse process $n\pi \to p + \bar{p}$ is not included in the transport model it is not clear how meaningful the final state effects (in the UrQMD phase) are for the antiparticle $\bar{v}_2$.

Note that in our calculation the difference between proton and anti-proton elliptic flow is caused solely by the nonzero net baryon number density, and chemical potential, and therefore a similar effects should be be observed for a finite isospin and net strangeness chemical potential at midrapidity [94] if included properly in the model. As discussed at the end of Sec. II the difference in the (elliptic) flow of particles and antiparticles is due to the different local weighting $\exp(-2\mu_i(x, y)/T(x, y))$ when evaluated over the hypersurface. We can assume that the chemical potentials μ_i have a different magnitude $-\mu_I < \mu_S < \mu_B$ and therefore we expect the effect becomes weaker for kaons and even more for pions. This is in fact the case for the experimental data, as π^- show more $\bar{v}_2$ than π^+ and K^+ more than K^-, where the difference is smallest for the pions. Since the isospin chemical potential is negative due to the higher abundance of neutron in the colliding nuclei, this also explains why, contrary to the protons, in case of the pions the elliptic flow of the antiparticle, i.e., π^-, is larger than that of the particle (π^+).

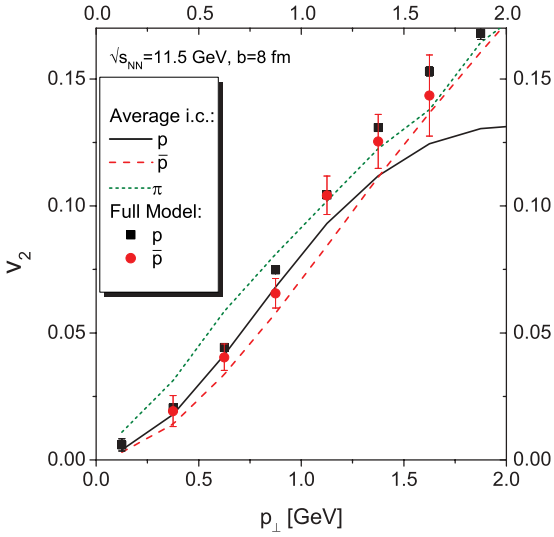

FIG. 11. (Color online) Elliptic flow of protons, anti-protons, and pions as a function of $p_\perp$. We show results from an averaged UrQMD initial state (lines) as well as from the full hybrid model calculations after the Cooper-Frye transition (no final state interaction) (symbols).

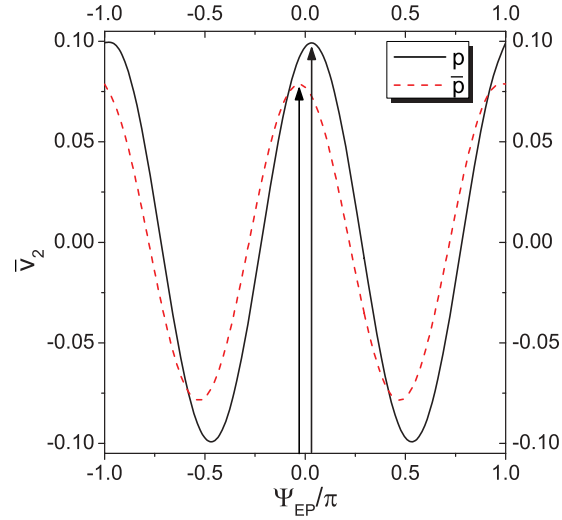

FIG. 12. (Color online) Integrated elliptic flow of protons and anti-protons for any given definition of the event plane angle $\Psi_{\rm EP}$.

In Fig. 2 we see that, during the hydrodynamical evolution, the average transverse momentum of $\bar{p}$ is smaller than that of p. Therefore, part of the difference in the integrated $\bar{v}_2$ can be understood as weighting $v_2(p_\perp)$ at higher values of $p_\perp$ in case of the protons [see Eq. (16)]. On the other hand the preliminary data by STAR indicate that also the differential elliptic flow parameter, $v_2(p_\perp)$, differs between protons and anti-protons. To investigate this in Fig. 11 we compare the differential elliptic flow for protons, anti-protons and pions after the Cooper-Frye transition. The lines represent results with the averaged initial conditions as described above, where we sampled the freeze-out hypersurface to obtain sufficient statistics. We indeed observe a small difference for $v_2(p_\perp)$ between $\bar{p}$ and p. From the event-by-event calculations we obtain results depicted as symbols. Here we also only observe a small difference, within the still considerable errors. In any case, in our calculation we find the effect due to the different $\langle p_\perp \rangle$ to be dominant.

Another effect which can artificially increase the observed asymmetry of baryon vs. anti-baryon elliptic flow, and in particular the difference in $p_\perp$ dependent v_2, may arise from the way v_2 is measured in experiment. While in our calculation the reaction plane is well defined, experiments have to reconstruct the so-called event plane in order to infer the reaction Pplane angle $\Psi_{\rm RP}$. This analysis method involves correlating the azimuthal angle ϕ of each particle with an event plane angle $\Psi_{\rm EP}$ which is defined by the other particles of that event [95]. Due to fluctuations, the event plane is usually not perfectly aligned with the reaction plane (see, e.g., [96]).

Furthermore, as a result of baryon number fluctuations an event plane direction, $\Psi_{\rm EP}^{[p]}$, defined only by protons may deviate from that defined solely by anti-protons, $\Psi_{\rm EP}^{[\bar{p}]}$. As a consequence, the elliptic flow for anti-protons calculated with respect to the event plane of the protons would be slightly smaller than if it were calculated with respect to the event plane of the anti-protons. To illustrate this we have plotted in Fig. 12 the integrated $\bar{v}_2$ for protons and anti-protons as a function of a trial event plane angle $\Psi_{\rm EP}$.[3] Obviously, for $\Psi_{\rm EP} = \Psi_{\rm EP}^{[p]}$ and $\Psi_{\rm EP} = \Psi_{\rm EP}^{[\bar{p}]}$ the values of $\bar{v}_2$ are maximal for protons and anti-protons, respectively, indicating the correct direction of the respective event planes. Furthermore, one can clearly see that the maxima for protons and anti-protons are separated by a finite angle.

Since at low collision energies protons are much more abundant than anti-protons, it is likely that the determination of the event plane is biased towards the direction of the proton event plane, $\Psi_{\rm EP}^{[p]}$. As a consequence, in each event the value extracted for v_2 of *anti-protons* will be less than the maximum, as shown in Fig. 11. Thus, the event averaged value for the integrated elliptic flow for anti-protons will be systematically smaller than that of protons, even if their true values would be the same.

At (nearly) vanishing net baryon densities this is not of importance because one has as many baryons as antibaryons and there is no bias towards either the proton or anti-proton event plane. In the case of baryon antibaryon asymmetry however, the event plane definition will always be biased towards the particle plane. In the energy range considered we estimated this effect to contribute to the difference of the flow by about 5–10%, by averaging the relative difference of the peak positions over many events. Note however, that this effect could be excluded if the event plane/reaction plane can be measured independently, e.g., from the spectator fragments, thus eliminating any bias.

V. SUMMARY

We have presented results calculated within the URQMD hybrid model for various observables from heavy ion

[3]The curves are obtained by calculating one event and evaluating $\bar{v}_2 = \langle \cos[2(\phi - \Psi_{\rm EP})] \rangle$ for values of $-\pi < \psi_{\rm EP} < \pi$.

collisions. The hybrid model is able to take into account the initial stopping, the explicit propagation of the baryon number, and the nonequilibrium transport in the hadronic phase, all of which are essential ingredients for studies of relativistic heavy ion collisions at large net baryon densities.

We find the observed nonmonotonic behavior of T_{eff} with hadron mass to be a direct consequence of the nonequilibrium transport in the hadronic phase. Observations like the centrality dependence of freeze-out parameters and the difference in particle and antiparticle spectra and elliptic flow, on the other hand, can, at least partially, be explained by the conservation of baryon charge.

We have argued that the observed difference in the elliptic flow between positively and negatively charged pions and kaons may likely be a consequence of the conserved net strangeness and isospin. Thus, future theoretical studies of heavy ion collisions at low energies should take into account the explicit conservation of these charges in addition to the baryon number conservation. We further pointed out that a transport treatment of the final hadronic phase should include both proton–anti-proton annihilation *and* production processes to ensure detailed balance. This is essential to draw firm conclusions about the physics leading to subtle difference between particle and antiparticle observables at low collision energies, such as the observed difference in the elliptic flow. Finally, we have pointed out that local fluctuations of the baryon number may lead to a biased determination of the event plane which may result in artificial differences between particle and antiparticle flow observables.

ACKNOWLEDGMENTS

The authors thank U. Heinz for fruitful discussions. This work was supported by BMBF, HGS-hire and the Hessian LOEWE initiative through the Helmholtz International center for FAIR (HIC for FAIR). J.S. acknowledges support by the Feodor Lynen program of the Alexander von Humboldt foundation. This work was supported by the Office of Nuclear Physics in the US Department of Energy's Office of Science under Contract No. DE-AC02-05CH11231. The computational resources were provided by the LOEWE Frankfurt Center for Scientific Computing (LOEWE-CSC).

[1] J. Y. Ollitrault, Phys. Rev. D **46**, 229 (1992).
[2] D. H. Rischke, Nucl. Phys. A **610**, 88c (1996).
[3] H. Sorge, Phys. Rev. Lett. **78**, 2309 (1997).
[4] H. Heiselberg and A. M. Levy, Phys. Rev. C **59**, 2716 (1999).
[5] S. Scherer *et al*., Prog. Part. Nucl. Phys. **42**, 279 (1999).
[6] S. Soff, S. A. Bass, M. Bleicher, H. Stoecker, and W. Greiner, arXiv:nucl-th/9903061.
[7] J. Brachmann *et al*., Phys. Rev. C **61**, 024909 (2000).
[8] L. P. Csernai and D. Rohrich, Phys. Lett. B **458**, 454 (1999).
[9] B. Zhang, M. Gyulassy, and C. M. Ko, Phys. Lett. B **455**, 45 (1999).
[10] P. F. Kolb, J. Sollfrank, and U. W. Heinz, Phys. Rev. C **62**, 054909 (2000).
[11] M. Bleicher and H. Stoecker, Phys. Lett. B **526**, 309 (2002).
[12] H. Stoecker, Nucl. Phys. A **750**, 121 (2005).
[13] X. Zhu, M. Bleicher, and H. Stöcker, Phys. Rev. C **72**, 064911 (2005).
[14] H. Petersen, Q. Li, X. Zhu, and M. Bleicher, Phys. Rev. C **74**, 064908 (2006).
[15] M. Gazdzicki *et al*. (NA49 Collaboration), J. Phys. G **30**, S701 (2004).
[16] M. Gazdzicki and M. I. Gorenstein, Acta Phys. Pol. B **30**, 2705 (1999).
[17] J. Adams *et al*. (STAR Collaboration), Nucl. Phys. A **757**, 102 (2005).
[18] B. B. Back *et al*., Nucl. Phys. A **757**, 28 (2005).
[19] I. Arsene *et al*. (BRAHMS Collaboration), Nucl. Phys. A **757**, 1 (2005).
[20] K. Adcox *et al*. (PHENIX Collaboration), Nucl. Phys. A **757**, 184 (2005).
[21] K. Aamodt *et al*. (ALICE Collaboration), Phys. Rev. Lett. **106**, 032301 (2011).
[22] K. Aamodt *et al*. (ALICE Collaboration), Phys. Lett. B **696**, 30 (2011).
[23] KAamodt *et al*. (ALICE Collaboration), Phys. Rev. Lett. **105**, 252302 (2010).
[24] BAbelev *et al*. (ALICE Collaboration), Phys. Rev. Lett. **105**, 252301 (2010).
[25] S. A. Bass *et al*., Prog. Part. Nucl. Phys. **41**, 255 (1998).
[26] M. Bleicher *et al*., J. Phys. G **25**, 1859 (1999).
[27] J. Geiss, W. Cassing, and C. Greiner, Nucl. Phys. A **644**, 107 (1998).
[28] W. Cassing and E. L. Bratkovskaya, Phys. Rep. **308**, 65 (1999).
[29] M. Bleicher, E. Bratkovskaya, S. Vogel, and X. Zhu, J. Phys. G **31**, S709 (2005).
[30] S. A. Bass and A. Dumitru, Phys. Rev. C **61**, 064909 (2000).
[31] D. Teaney, J. Lauret, and E. V. Shuryak, arXiv:nucl-th/0110037.
[32] T. Hirano, U. W. Heinz, D. Kharzeev, R. Lacey, and Y. Nara, Phys. Lett. B **636**, 299 (2006).
[33] C. Nonaka and S. A. Bass, Phys. Rev. C **75**, 014902 (2007).
[34] P. Romatschke and U. Romatschke, Phys. Rev. Lett. **99**, 172301 (2007).
[35] T. Hirano, P. Huovinen, and Y. Nara, Phys. Rev. C **84**, 011901(R) (2011).
[36] B. Schenke, S. Jeon, and C. Gale, Phys. Lett. B **702**, 59 (2011).
[37] H. Petersen, Phys. Rev. C **84**, 034912 (2011).
[38] V. K. Magas, L. P. Csernai, and D. Strottman, arXiv:hep-ph/0110347.
[39] S. Paiva, Y. Hama, and T. Kodama, Phys. Rev. C **55**, 1455 (1997).
[40] C. E. Aguiar, Y. Hama, T. Kodama, and T. Osada, Nucl. Phys. A **698**, 639 (2002).
[41] O. Socolowski, Jr., F. Grassi, Y. Hama, and T. Kodama, Phys. Rev. Lett. **93**, 182301 (2004).
[42] T. Hirano, U. W. Heinz, D. Kharzeev, R. Lacey, and Y. Nara, Phys. Rev. C **77**, 044909 (2008).
[43] S. A. Bass, A. Dumitru, M. Bleicher, L. Bravina, E. Zabrodin, H. Stöcker, and W. Greiner, Phys. Rev. C **60**, 021902(R) (1999).
[44] A. Dumitru, S. A. Bass, M. Bleicher, H. Stoecker, and W. Greiner, Phys. Lett. B **460**, 411 (1999).
[45] B. Schenke, S. Jeon, and C. Gale, Phys. Rev. C **82**, 014903 (2010).

[46] Z. W. Lin, C. M. Ko, B. A. Li, B. Zhang, and S. Pal, Phys. Rev. C **72**, 064901 (2005).
[47] W. Cassing and E. L. Bratkovskaya, Nucl. Phys. A **831**, 215 (2009).
[48] W. Cassing and E. L. Bratkovskaya, Phys. Rev. C **78**, 034919 (2008).
[49] H. Petersen, J. Steinheimer, G. Burau, M. Bleicher, and H. Stocker, Phys. Rev. C **78**, 044901 (2008).
[50] J. Steinheimer, M. Bleicher, H. Petersen, S. Schramm, H. Stocker, and D. Zschiesche, Phys. Rev. C **77**, 034901 (2008).
[51] D. H. Rischke, S. Bernard, and J. A. Maruhn, Nucl. Phys. A **595**, 346 (1995).
[52] D. H. Rischke, Y. Pursun, and J. A. Maruhn, Nucl. Phys. A **595**, 383 (1995); **596**, 717(E) (1996).
[53] H. Petersen, J. Steinheimer, M. Bleicher, and H. Stocker, J. Phys. G **36**, 055104 (2009).
[54] J. Steinheimer, V. Dexheimer, M. Bleicher, H. Petersen, S. Schramm, and H. Stöcker, Phys. Rev. C **81**, 044913 (2010).
[55] Q. f. Li, J. Steinheimer, M. Bleicher, H. Petersen, and H. Stocker, Phys. Lett. B **674**, 111 (2009).
[56] F. Cooper and G. Frye, Phys. Rev. D **10**, 186 (1974).
[57] F. Becattini, M. Gazdzicki, A. Keranen, J. Manninen, and R. Stock, Phys. Rev. C **69**, 024905 (2004).
[58] A. Andronic, P. Braun-Munzinger, and J. Stachel, Phys. Lett. B **673**, 142 (2009); **678**, 516(E) (2009).
[59] J. Cleymans, H. Oeschler, K. Redlich, and S. Wheaton, Phys. Rev. C **73**, 034905 (2006).
[60] H. Petersen, J. Steinheimer, Q. Li, G. Burau, and M. Bleicher, arXiv:0806.1805 [hep-ph].
[61] J. Steinheimer, H. Petersen, M. Mitrovski, and M. Bleicher, J. Phys. G **37**, 094038 (2010).
[62] E. Santini, J. Steinheimer, M. Bleicher, and S. Schramm, Phys. Rev. C **84**, 014901 (2011).
[63] J. Steinheimer and M. Bleicher, Phys. Rev. C **84**, 024905 (2011).
[64] J. Steinheimer, K. Gudima, A. Botvina, I. Mishustin, M. Bleicher, and H. Stocker, Phys. Lett. B **714**, 85 (2012).
[65] P. Huovinen and H. Petersen, arXiv:1206.3371 [nucl-th].
[66] P. Braun-Munzinger, I. Heppe, and J. Stachel, Phys. Lett. B **465**, 15 (1999).
[67] J. P. Blaizot and J. Y. Ollitrault, Adv. Ser. Direct. High Energy Phys. **6**, 393 (1990).
[68] L. Kumar (STAR collaboration), arXiv:1201.4203 [nucl-ex].
[69] J. Sollfrank, P. Koch, and U. W. Heinz, Phys. Lett. B **252**, 256 (1990).
[70] N. Xu and M. Kaneta, Nucl. Phys. A **698**, 306 (2002).
[71] A. Dumitru, L. Portugal, and D. Zschiesche, Phys. Rev. C **73**, 024902 (2006).
[72] N. Arbex, F. Grassi, Y. Hama, and O. Socolowski, Phys. Rev. C **64**, 064906 (2001).
[73] G. E. Brown, J. Stachel, and G. M. Welke, Phys. Lett. B **253**, 19 (1991).
[74] W. Florkowski, W. Broniowski, and M. Michalec, Acta Phys. Pol. B **33**, 761 (2002).
[75] S. V. Afanasiev *et al.* (NA49 Collaboration), Phys. Rev. C **66**, 054902 (2002).
[76] C. Alt *et al.* (NA49 Collaboration), Phys. Rev. C **73**, 044910 (2006).
[77] C. Alt *et al.* (NA49 Collaboration), Phys. Rev. Lett. **94**, 192301 (2005).
[78] L. P. Csernai, V. K. Magas, E. Molnar, A. Nyiri, and K. Tamosiunas, Eur. Phys. J. A **25**, 65 (2005).
[79] E. Molnar, L. P. Csernai, V. K. Magas, A. Nyiri, and K. Tamosiunas, Phys. Rev. C **74**, 024907 (2006).
[80] E. Molnar, L. P. Csernai, V. K. Magas, Z. I. Lazar, A. Nyiri, and K. Tamosiunas, J. Phys. G **34**, 1901 (2007).
[81] H. Sorge, Phys. Rev. Lett. **82**, 2048 (1999).
[82] C. M. Hung and E. V. Shuryak, Phys. Rev. Lett. **75**, 4003 (1995).
[83] J. Brachmann, A. Dumitru, H. Stoecker, and W. Greiner, Eur. Phys. J. A **8**, 549 (2000).
[84] P. F. Kolb, J. Sollfrank, and U. W. Heinz, Phys. Lett. B **459**, 667 (1999).
[85] J. Y. Ollitrault, Nucl. Phys. A **638**, 195 (1998).
[86] A. Schmah (STAR Collaboration), J. Phys. G **38**, 124049 (2011).
[87] J. Xu, L. W. Chen, C. M. Ko, and Z. W. Lin, Phys. Rev. C **85**, 041901(R) (2012).
[88] B. Abelev *et al.* (ALICE Collaboration), arXiv:1208.1974 [hep-ex].
[89] J. Steinheimer, J. Aichelin, and M. Bleicher, arXiv:1203.5302 [nucl-th].
[90] W. Cassing, Nucl. Phys. A **700**, 618 (2002).
[91] R. Rapp and E. V. Shuryak, Phys. Rev. Lett. **86**, 2980 (2001).
[92] C. Greiner and S. Leupold, J. Phys. G **27**, L95 (2001).
[93] R. Rapp, Phys. Rev. C **66**, 017901 (2002).
[94] J. Steinheimer, M. Mitrovski, T. Schuster, H. Petersen, M. Bleicher, and H. Stoecker, Phys. Lett. B **676**, 126 (2009).
[95] K. H. Ackermann *et al.* (STAR Collaboration), Phys. Rev. Lett. **86**, 402 (2001).
[96] H. Petersen, G. Y. Qin, S. A. Bass, and B. Muller, Phys. Rev. C **82**, 041901(R) (2010).